# Wound induced auxin accumulation and *ERF115* expression synergistically drive stem cell regeneration

Balkan Canher[1,2], Jefri Heyman[1,2], Maria Savina[3,4], Ajay Devendran[5], Thomas Eekhout[1,2], Ilse Vercauteren[1,2], Els Prinsen[6], Rotem Matosevich[7], Jian Xu[8], Victoria Mironova[3,4] and Lieven De Veylder[1,2,*]

[1]Department of Plant Biotechnology and Bioinformatics, Ghent University, Ghent, B-9052, Belgium
[2]VIB Center for Plant Systems Biology, Ghent, B-9052, Belgium
[3]Institute of Cytology and Genetics SB RAS, Novosibirsk 630090, Russia
[4]Novosibirsk State University, Novosibirsk 630090, Russia
[5]Department of Biological Sciences and Centre for BioImaging Sciences, National University of Singapore, Singapore 117543, Singapore
[6]Integrated Molecular Plant Physiology Research (IMPRES), Department of Biology, University of Antwerp, Groenenborgerlaan 171, 2020, Antwerp, Belgium
[7]Institute of Plant Sciences and Genetics in Agriculture, Faculty of Agriculture, The Hebrew University of Jerusalem, Rehovot, Israel
[8]Department of Plant Ecology and Physiology, Faculty of Science, Radboud University, 6525 AJ Nijmegen, Netherlands
* Corresponding author: De Veylder, Lieven

**Email:** lieven.deveylder@psb.vib-ugent.be

**This PDF file includes:**

Supplementary text
Figures S1 to S7
Tables S1 to S3
Legend for Movies S1 to S2
Legend for Datasets S1
SI References

**Other supplementary materials for this manuscript include the following:**

Movies S1 to S2
Dataset S1



www.pnas.org/cgi/doi/10.1073/pnas.2006620117

**Supplementary Information Text**

**Bleomycin Recovery Experiments**

For BLM (Calbiochem) treatment, seedlings were transferred 5 days after germination in vertical plates supplemented with 0.6 µg/mL BLM. For recovery, seedlings were retransferred to control medium after 1 day of growth on BLM-containing medium and allowed to recover for 6 days. Root lengths were analyzed with ImageJ 1.41 software (http://rsb.info.nih.gov/ij/) and total root elongation was calculated. Because seedlings with collapsed root meristems following BLM treatment tended to show in general a root elongation that was smaller than 0.5 cm over 6 days of recovery, seedlings with < 0.5 cm root growth were scored as failed recovery. Probability of successful recovery (> 0.5 cm growth) was statistically compared using logistic regression analysis in SAS Enterprise Guide 7.15 HF8. Recovery or collapse were modeled as binary response and the model was fit to level=1, representing successful recovery. Genotype and independent repeats were included as main effects and odds ratios with Wald confidence limits (%95) and P-values were calculated. Statistical analysis for total root elongation under control conditions was performed using mixed model analysis with least squares post-hoc tests and corrected for multiple pairwise comparisons using the Tukey method.

**Treatments**

For germination for the NPA experiments, 125 mM NPA stock in DMSO was diluted to a final concentration of 10 µM in ½ MS agar medium. Seedlings were germinated and grown on NPA medium for indicated times. For quantification of the amyloplast-accumulating area, seedlings were stained with Lugol solution and imaged by light microscopy. The height of the region containing darkly stained amyloplasts was measure in ImageJ. Statistical analysis was executed with the Statistical Analysis Software (SAS Enterprise Guide 5.1; SAS Institute, Inc.) using the mixed model procedure by least squares post-hoc tests and corrected for multiple pairwise comparisons using the Tukey method. Genotype was added as a main effect and estimates were calculated by Residual Maximum Likelihood. Experimental repeats were included as random effect. Degrees of freedom were calculated by the Kenward-Rogers method.

For IAA and MeJA treatments, seedlings were treated with on ½ MS agar medium containing either 1uM IAA or 1uM IAA and 50µM MeJA for 24 hours. Hydrogen Peroxide treatments were performed in liquid 1/2MS medium at 0.5mM or 1mM concentration and fixed immediately for GUS staining.

**GUS Staining**

GUS staining was performed by fixation in 80% aceton for 30min, followed by 3 washes with Phosphate Buffer (pH7.2). Seedlings were stained overnight at 37°C in GUS staining buffer (2mM Potassium Ferricyanide, 2mM Potassium Ferrocyanide and 0.5g/L X-Gluc).

previously31. Following staining, samples were washed 3 times with phosphate buffer and cleared in a 75:25% ethanol/acetic acid solution before mounting on slides using lactic acid.

**Pseudo Schiff Propidium Iodide (mPS-PI) Staining**

Seedlings were fixed in a solution containing 50%methanol and 10% acetic acid at 4°C overnight. Fixed seedlings were rinsed with water and incubated in 1% periodic acid at room tempterature for 40min. After rinsing with water, seedlings were stained with freshly prepared Schiff Reagent (100mM sodium metabisulfite, 0.15N HCl, 100µg/ml Propidium Iodide) until the roots were visibly stained red. Samples were then mounted on microscope slides with chloral hydrate solution (4g chloral hydrate, 1ml glycerol and 2ml water) and imaged.

**mRNA Extraction and qRT-PCR**

RNA was isolated from the root tips of 5-d-old Col-0 and *35S:ERF115-SRDX* seedlings treated with BLM for 24 h or not with the RNeasy Plant Mini kit (Qiagen). DNase treatment was done with the RQ1 RNase-Free DNase (Promega) prior to cDNA synthesis with the iScript cDNA Synthesis kit (Bio-Rad). Relative expression levels were determined by quantitative reverse-transcription polymerase chain reaction (qRT-PCR) with the LightCycler 480 Real-Time SYBR Green PCR System (Roche). Three different reference genes were used for normalization: *ACT*, *CAK2* and *EMB2386*. Primer sequences used for qRT-PCR analyses are given in Table S2. Statistical analysis was performed using a 2-tailed Student's t-test.

**RNA-Seq**

Five days old seedlings (2days of vernelization and 5 days in the growth chamber) were transferred on mesh to either fresh control medium or medium supplemented with 0.5 µg/ml BLM (Calbiochem) for 24 h. Root tips (around 2 mm) were collected in liquid nitrogen in three biological repeats. RNA was extracted using the RNEasy Plant Mini kit (Qiagen) and Illumina Tru-Seq libraries were generated from cDNA and sequenced on a NextSeq500 75-bp single-end run. All analyses were done using the Galaxy platform. Reads were filtered and trimmed, after which transcript quantification was performed by Salmon version 0.7.2 (1) using the Araport11 exome, with all parameters set to default values. Transcript quantification results generated by Salmon were corrected for gene length variations across the samples using the tximport 1.6.0 R package (2) and were further analyzed using the DESeq2 package (3). Transcripts with a read count of less than ten in all samples combined were removed from further analyses. Normalized read counts were $\log_2$ transformed, and a negative binomial generalized linear model was fitted to the data using the treatment as the factor to identify differential gene expression. The significance of the expression changes was determined using Wald tests and corrected for multiple testing by the Benjamini-Hochberg method (4).

**Confocal and Light Microscopy**

Arabidopsis roots were stained using propidium iodide (PI) by incubation in a 10-μM solution for 3 min before imaging. For confocal microscopy, a Zeiss LSM5 Exciter Confocal was used. GFP fluorescence was observed after excitation using a 488-nm laser and detected using the bandpass 505–530-nm emission filter setting. PI fluorescence was observed after excitation using a 543-nm laser and detected using the 650-nm long-pass emission filter. Ratiometric quantifications on R2D2 images were performed in FIJI Win64 64bit edition (Downloaded on 2017 May 30) by measuring mean gray values of green and red nuclear signals on confocal images. Imaging was performed on a Leica TCS SP8 X microscope equipped with Argon laser (488 nm) for GFP excitation and White Light Laser (554 nm) for tdTomato excitation. GFP and tdTomato emissions were collected at 500-540 nm and 570-630 nm, respectively. For light and DIC microscopy, an Olympus BX51 microscope was used. For Technovit sectioning, NPA- or mock-treated seedlings were fixed in a paraformaldehyde(4%)-gluteraldehyde(1%) solution, dehydrated through a graded ethanol series and embedded in Technovit 7100 (Heraeus Kulzer). Sections of 4-μm thickness were prepared and counterstained as described in De Smet*, et al.* (5).

**Mathematical Modeling of Auxin Distribution**

We used the PlantLayout pipeline for MatLab© to build a series of mathematical models with realistic root tip layout to study auxin patterning after BLM treatment (6). First, we created a structural model of the two-dimensional root tip tissue; second, an existing mathematical model of auxin patterning in ordinary differential equations (ODEs) (7, 8) was embedded into the layout; third, we imitated BLM treatment by introducing dead cells into the layout; fourth, we adjusted the model parameters and performed numerical simulations. The details are provided below:

***Step 1. A two-dimensional structural model of the Arabidopsis root tip***

Starting from a preprocessed microscopic image of a real Arabidopsis root tip, the PlantLayout pipeline (6) built a two-dimensional structural model. PlantLayout applies the *bwconncomp* function from MATLAB Image Processing Toolbox to identify all cells and cell walls as connected components within the preprocessed image. The cells from the layout receive unique index numbers from 1 to $N$+2, where 3 to $N$+2 corresponds to the root cells and indexes 1 and 2 identify the environment and the non-modeled part of the root (above the cell layout), respectively. The structural model contains the following quantitative and qualitative characteristics of the longitudinal cut of the real root tip: (1) the size of each cell (the area and the perimeter); (2) the size of each cell wall between any two adjacent cells (length and width); (3) the orientation of the cell walls (1 - “top”, 2 - “bottom”, 3 - “right”, 4 - “left”) for each cell. We annotated the following cell types in the model: root cap, QC, columella stem cells, epidermis, cortex endodermis and the vasculature.

***Step 2. Two-dimensional mathematical model of auxin distribution within the root meristem***

We used an existing mathematical model of auxin transport in the root meristem described in Hong*, et al.* (7) and Mironova*, et al.* (8) with some modifications and embedded it into the two-dimensional structural model with the PlantLayout help.

The model considers the following processes: auxin synthesis, degradation, diffusion, PIN-mediated active transport, and auxin-dependent expression of PINs. There are three generalized PINs in the model: PIN1347 that combines the function of four auxin transporters with the rootward and lateral polarities (PIN1, PIN3, PIN4, PIN7) in the proximal meristem; PIN2 that reflects the function of PIN2 in the outer layers; PIN347 that combines the function of three proteins with nonpolar localization (PIN3, PIN4, PIN7) in the distal meristem (6). We assigned these generalized proteins to specific cell types. Stele, endodermis, QC, and CSC are able to express PIN1347 with rootward and lateral polarity. Cortex and epidermis cells are able to express PIN2, cortex with the rootward and lateral polarities, epidermis with shootward, and lateral polarities. We modified the description of PIN347 expression domain comparing with the original model (7, 8). Only root cap cells, QC and CSC are able to express PIN347 that transports auxin non-polarly. As in the initial model (8), the rates of PIN1347, PIN2, PIN347 synthesis and the rates of PIN1347, PIN2 degradation in a cell depend on the internal auxin level.

Each of the lateral auxin flows in the vascular, QC, and CSC cells reached 20% of the total PIN1347 mediated auxin flow in these cells. Thus, the rootward auxin flow in these cells was 60% of the total PIN1347-mediated auxin flow. Lateral auxin flow in endodermis, cortex, and epidermis reached 20% of the total PIN1347/PIN2 mediated auxin flows in these cells. The rest 80% of the total PIN1347/PIN2-mediated auxin flow was set for either rootward flow in endodermis and cortex, or shootward flow in the epidermis.

We adapted the system of ordinary differential equations (ODE) describing the dynamics of four variables into each cell ($[a]_i$, $[PIN1347]_i$, $[PIN2]_i$, $[PIN347]_i$) to take into account different cell sizes and cell wall lengths (Eq. 1)

$$\begin{cases} \dfrac{d[PIN1347]_i}{dt} = \left( K_{s,PIN1347} \dfrac{\left(\dfrac{[a]_i}{q_{1,PIN1347}}\right)^{s_{PIN1347}}}{1+\left(\dfrac{[a]_i}{q_{2,PIN1347}}\right)^{s_{PIN1347}}} - K_{d,PIN1347}\left(1+\left(\dfrac{[a]_i}{q_{3,PIN1347}}\right)^{h_{PIN1347}}\right) \times [PIN1347]_i \right) \dfrac{1}{V_i} \\ \dfrac{d[PIN2]_i}{dt} = \left( K_{s,PIN2} \dfrac{\left(\dfrac{[a]_i}{q_{1,PIN2}}\right)^{s_{PIN2}}}{1+\left(\dfrac{[a]_i}{q_{2,PIN2}}\right)^{s_{PIN2}}} - K_{d,PIN2}\left(1+\left(\dfrac{[a]_i}{q_{3,PIN2}}\right)^{h_{PIN2}}\right) \times [PIN2]_i \right) \dfrac{1}{V_i} \\ \dfrac{d[PIN347]_i}{dt} = \left( K_{s,PIN347} \dfrac{\left(\dfrac{[a]_i}{q_{1,PIN347}}\right)^{s_{PIN347}}}{1+\left(\dfrac{[a]_i}{q_{2,PIN347}}\right)^{s_{PIN347}}} - K_{d,PIN347} \times [PIN347]_i \right) \dfrac{1}{V_i} \\ \dfrac{d[a]_i}{dt} = \left( k_\alpha * p_i + K_{s,a}(i) - K_{d,a}[a]_i + D \times \sum_{m \in N_i} \left( ([a]_m - [a]_i) l_{i,m} \right) + \sum\nolimits_{x \in P} J_x(i) \right) \dfrac{1}{V_i} \end{cases},$$

(1)

, where $k_\alpha$ is the intensity of auxin flow from the elongation zone to the meristem; $p_i$ is the fraction of auxin flow from the elongation zone per cell *i*; $K_{s,a}(i)$ is the auxin biosynthesis rate constant; $K_{d,a}$ is the auxin degradation rate constant; *D* is the auxin diffusion rate constant; $N_i$ is the set of neighboring cells for the cell *i*; $J_x(i)$ represents the auxin flows mediated by PINs, where x denotes PIN1347, PIN2, PIN347; $K_{s,x}$ is the synthesis rate constant; $q_{1,x}$ is the activation thresholds of auxin-dependent PIN protein synthesis; $q_{2,x}$ is the saturation thresholds of auxin-dependent PIN protein synthesis; $s_x$ is the Hill coefficient, which determines the rate of PIN protein synthesis in response to changes in intracellular auxin concentration; $K_{d,x}$ is the degradation rate constant; $q_{3,x}$ is the thresholds of auxin-dependent PIN protein degradation; $h_x$ are the coefficients that define non-linearity of auxin-regulated PIN protein degradation.; $V_i$ is the volume of the cell *i* (in the 2-dimensional case – the cross-section area); $l_{i,m}$ is the length of the cell wall between cells *i* and *m*. We took into account only TAA1-dependent auxin synthesis in the QC and CSC cells ($K_{s,a}(i)$ in Table S1). No regulation of auxin synthesis after BLM treatment was considered, according to the experimental data.

The primary source of auxin in the cell layout is the auxin flow from the elongation zone, which is assigned for the upper vasculature cells only (neighboring to the index 2 space):

$$p_i = \frac{l_{i,2}}{\sum_j l_{j,2}} \quad (2)$$

where $l_{i,2}$ is the length of the cell wall between cells *i* and 2; $\sum_j l_{j,2}$ is the total length of all cell walls of the stele and endodermis bordering the index 2 space.

The auxin flows mediated by PINs were determined by the distribution of auxin flows described above:

$$J_x(i) = \sum_{m \in N_i} \left( k^x_{m,i}[a]_m[x]_m - k^x_{i,m}[a]_i[x]_i \right), \quad (3)$$

where $N_i$ is the set of neighboring cells for the cell *i*; $k_{m,i}^x$ is the constant reflecting the fraction of the protein *x* located on the membrane of the cell *m* neighboring to cell *i* from the total protein *x* in cell *m*; $k_{i,m}^x$ is the constant reflecting the fraction of the protein *x* located on the membrane of cell *i* neighboring to the cell *m* relative to the total protein *x* in cell *i*; *x*∈{*PIN*1, *PIN*2, *PIN*3}.

Parameters $V_i$, $l_{i,j}$, $k_{i,j}^{PIN1}$, $k_{i,j}^{PIN2}$, $k_{i,j}^{PIN3}$, $k_{i,j}^{PIN4}$, $k_{i,j}^{PIN7}$ and $p_i$ were defined by the PlantLayout in the structural model.

***Step 3. Adjusting the parameter settings***

Most parameters of the model were either inherited from the previous model (7) or taken from the structural model (generated in the step 1).

The parameters for auxin-dependent PIN synthesis and PIN degradation were adjusted according to the following rules:

- The QC and columella must have the auxin maximum in the steady-state solution;
- Distribution of all PINs in the steady-state solution must match the experimentally observed generalized domains having the same polarity;
- The ratio between auxin maximum and average auxin concentration in the endodermis in the steady-state solution must be less than ten times.

The full set of the parameter values listed in Table S1 was used to obtain the steady-state solution for the control (Fig. S4).

***Step 4. Simulation of BLM treatment***

To simulate cell death after BLM treatment, we removed all differential equations that corresponded to the dead cells from the ODE system for control. Besides, we removed all flows of auxin diffusion and auxin active transport between the dead cells and their neighbors. Based on experimental images after BLM treatment, we built ten models simulating auxin transportation in the injured root tips (Fig. S3).

To simulate BLM treatment, we used steady-state solution for control as initial data. We reduced PIN1347 synthesis rate constant ($K_{s,PIN1347}$) by 33% according to the experimental data on the changes of fluorescent intensity in PIN1::PIN1-GFP root tips after 24 hours of BLM treatment (Table S1). We also fixed PIN2 and PIN347 expression patterns as the fluorescent intensity in PIN2::PIN2-GFP, PIN3::PIN3-GFP and PIN4::PIN4-GFP levels in root tips have not changed significantly (Fig. S4). In an alternative study, we left the levels of all PINs unchanged to see the contribution coming from the reduction in PIN levels (Fig. S6).

Then we calculated each of ten models imitating BLM treatment till the steady-state. For visualization of the model results (Fig. 4E, F, Fig. S5, 6), we estimated the difference in auxin and PINs concentrations between control and BLM treated root tips.

***Step 5. Variation in the PIN1347 synthesis rate value.***

To obtain the "confidence" interval for the model simulation we performed the variation of the PIN1347 synthesis rate constant ($K_{s,PIN1347}$) in the model within the maximal deviation interval averaged for the experimentally observed GFP signals in the lines PIN1::PIN1-GFP, PIN3::PIN3-GFP, and PIN4::PIN4-GFP after 24 hours of BLM treatment (Fig. S4). Namely, of the PIN1347 synthesis rate constant ($K_{s,PIN1347}$) were varied between the 60% and the 89% of control value with the 1% step.

**Calculation of Maximal Error**

To calculate the maximal error, four ratios were calculated for each cell positon based on mean (MEAN) auxin concentration (for model) or Red/Green ratio (R2D2) :

$Ratio1 = (MEAN_{BLM} - StDev_{BLM})/(MEAN_{CNTRL} - StDev_{CNTRL})$;
$Ratio2 = (MEAN_{BLM} - StDev_{BLM})/(MEAN_{CNTRL} + StDev_{CNTRL})$;
$Ratio3 = (MEAN_{BLM} + StDev_{BLM})/(MEAN_{CNTRL} - StDev_{CNTRL})$;
$Ratio4 = (MEAN_{BLM} + StDev_{BLM})/(MEAN_{CNTRL} + StDev_{CNTRL})$;

$MaximalError\_down = MEAN_{BLM}/MEAN_{CNTRL} - MIN(ratio1, ratio2, ratio3, ratio4)$

$MaximalError\_up = MAX(ratio1, ratio2, ratio3, ratio4) - MEAN_{BLM}/MEAN_{CNTRL}$

**Analysis of Auxins**

Homogenized plant samples (100 mg) were extracted in 500 µl 80% MeOH. 300 pmol [13C6]-IAA [(phenyl-13C6)-indole-3-acetic acid, 99%, Cambridge Isotopes, USA] was added as internal tracer. After overnight extraction, samples were centrifuged (15,000 g, 4°C, 20 min, Eppendorf 5810R, Eppendorf AG, Hamburg, Germany) and the supernatant was aliquoted in two equal parts. One aliquot was acidified using 5 ml 6% formic acid and concentrated on a RP-C18 cartridge (500 mg, BondElut Varian, Middelburg, The Netherlands). Auxins were eluted with 5 ml diethylether and dried under nitrogen (TurboVap® LV Evaporator, Zymarck). A second aliquot was hydrolyzed in 7 M NaOH for 3 h at 100°C under water-saturated nitrogen atmosphere to hydrolyze all ether as well as ester conjugates (9). After hydrolysis, the samples were acidified using 2 M HCl, concentrated on a C18 cartridge, and eluted with diethylether as described before. All samples were methylated using etheral diazomethane (10) to improve sensitivity, and analyzed as their corresponding methyl esters. Conjugates were analyzed as free compounds after acidification of this hydrolysis and after subtraction of the free aliquot after acidification of this hydrolysis.

Samples were analyzed using an Acquity UPLC system linked to a TQD triple quadrupole detector (Waters, Milford, MA) equipped with an electrospray interface in positive mode (UPLC-ESI-MS/MS). Samples (6 µl) were injected on an Acquity UPLC BEH C18 reversed-phase column (1.7 µm, 2.1 x 50 mm, Waters, Milford, MA) and eluted with a gradient of 1 mM ammonium acetate (A)/Methanol (B) at 0.3 ml min-1, 0-2 min isocratic 95%A/5%B, 2-4 min gradient to 10%A/90%B, 4-6 min isocratic 10%A/90%B. The effluent was introduced into the electrospray source (source temperature 140°C, capillary voltage 1,6 kV). Quantification was done by multiple reactant monitoring (MRM) of selected transitions based on the MH+ ion (dwell time 0,025) and the most appropriate compound-specific product ions (IAA-Me: 190>130, cone 18V, CE 18 eV; 13C6-IAA-Me: 196>136, 18V,18eV). All data were processed using Masslynx/Quanlynx software V4.1 (Waters, Milford, MA).

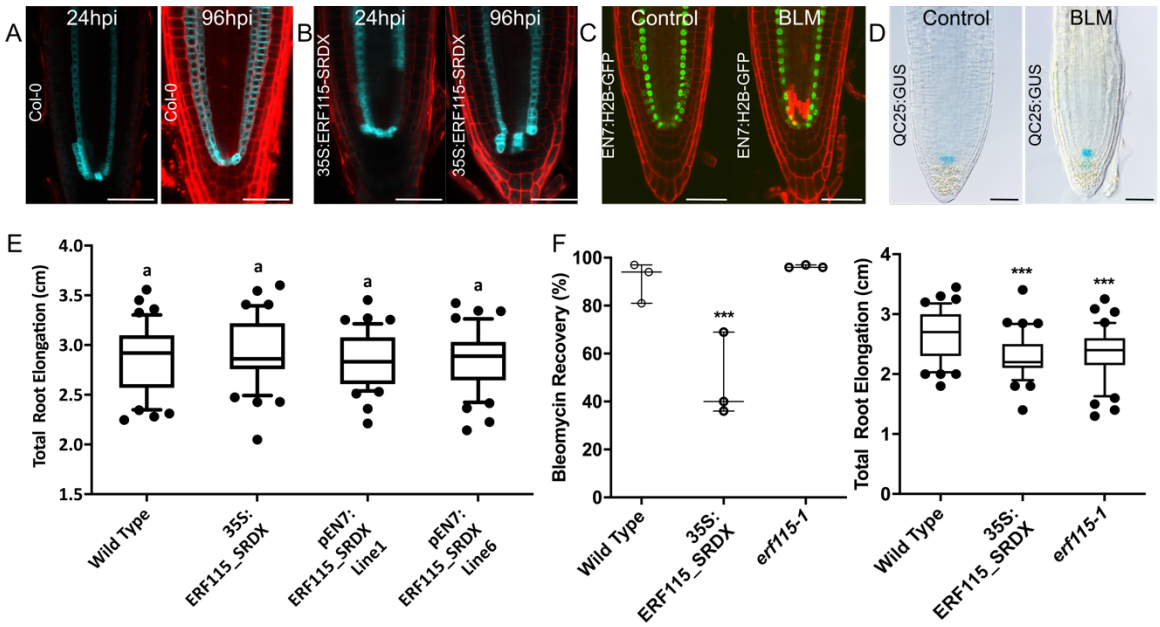


**Fig. S1.** (A,B) Confocal images of a *pSCR:CRE-GR 35S:loxp-tOCS-loxp-CFP* seedling in wild type (A) or *35S:ERF115-SRDX* (B) mutant background, 24 h or 96 h after DEX induction without BLM treatment. (hpi: hours post induction) (C) Confocal images of an *EN7:H2B-GFP* seedling with or without BLM treatment. (C) *QC25:GUS* seedlings with or without BLM treatment (E) Total root elongation of non-treated *EN7:ERF115-SRDX* seedlings over 6 days. Box plots represent data 10-90% percentile. Same letters represent statistical indifference (a equals to p>0.05). (F) BLM recovery ratios of *erf115-1* T-DNA mutant, *35S:ERF115-SRDX* dominant negative mutant and wild type(left panel) along with root elongation measurements under control conditions (right panel). (**, P<0.01, ***, P<0.001) Scale bars = 50 µm..

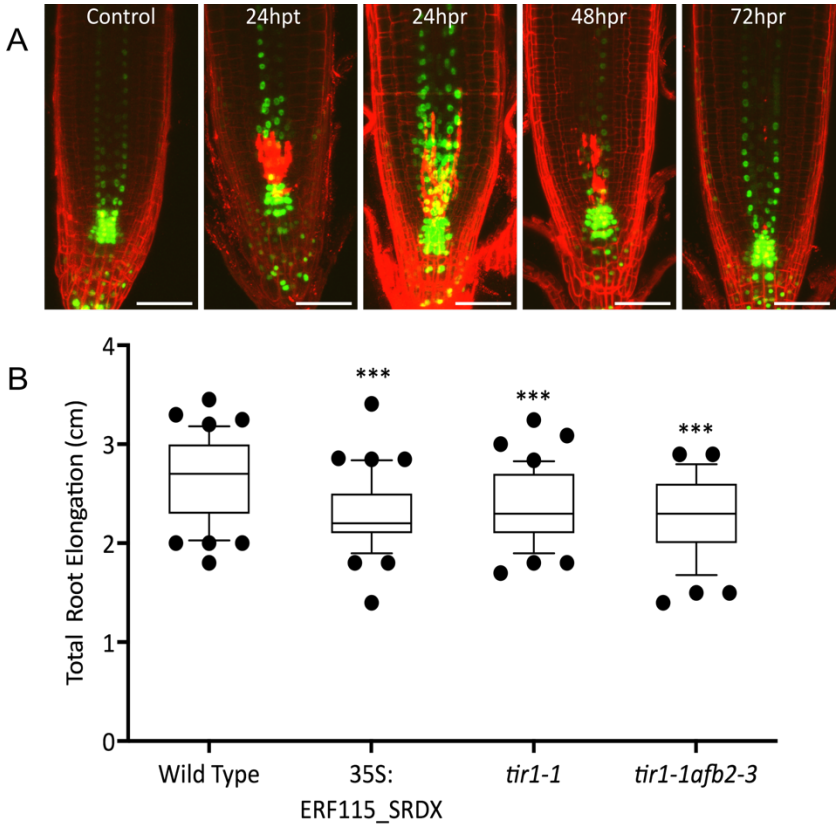


**Fig. S2** (A) Confocal images of PI stained *DR5:Venus-NLS* under control conditions and during BLM recovery for indicated times (hpt: hours post treatment, hpr: hours post recovery). Images represent maximum intensity projections from ten slices acquired with 1.5-µm intervals. (B) Total root elongation under control conditions (***P<0.001). Statistical analysis was performed as described in Fig. S1E.

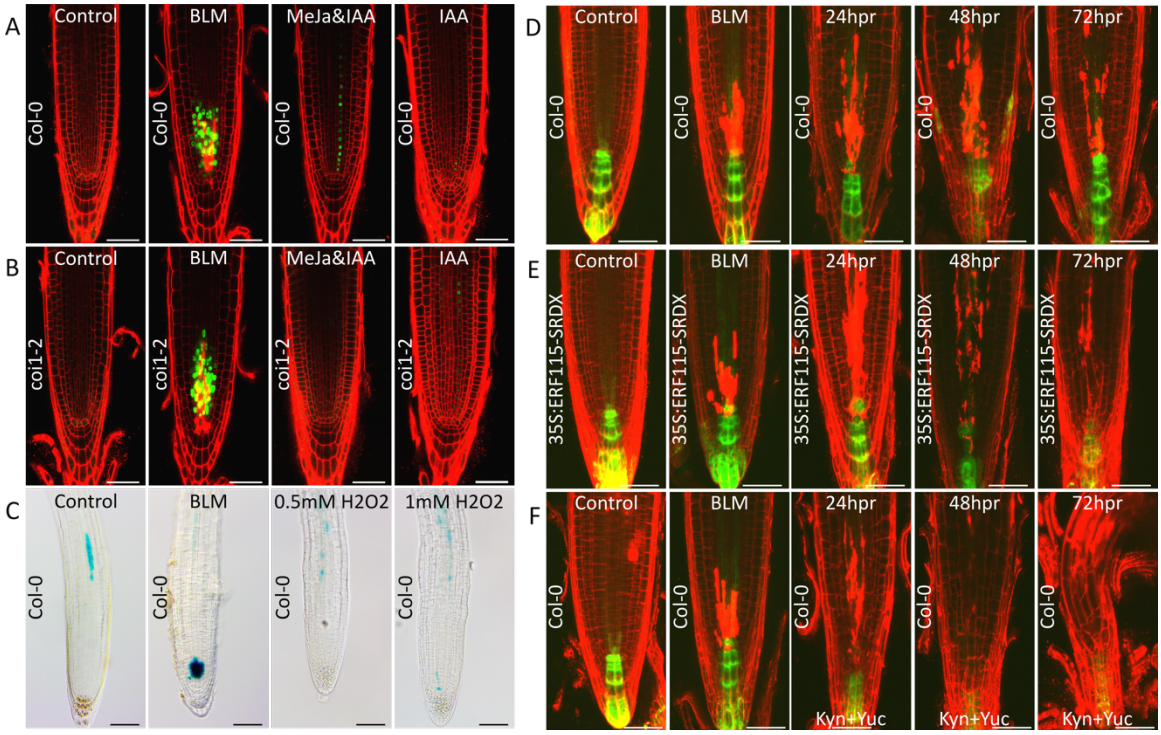


**Fig. S3.** (A,B) Confocal images of *ERF115:GFP-GUS* seedlings in the wild-type (A,C) or *coi1*-2 (B) background treated with indicated compounds for 24 h. (C) DIC images of GUS-stained *ERF115:GFP-GUS* seedlings following treatment with indicated compounds for 24 h. (D-E) Confocal images of PI stained (red) *DR5_GFP* (D-F) seedlings in wild-type (D,F) or *35S:ERF115-SRDX* (E) background treated for 24 h with BLM and recovered on normal medium (D,E) or auxin biosynthesis inhibitors 1uM kynurenine and 50uM yucasin (F). Scale bars = 50 μm.

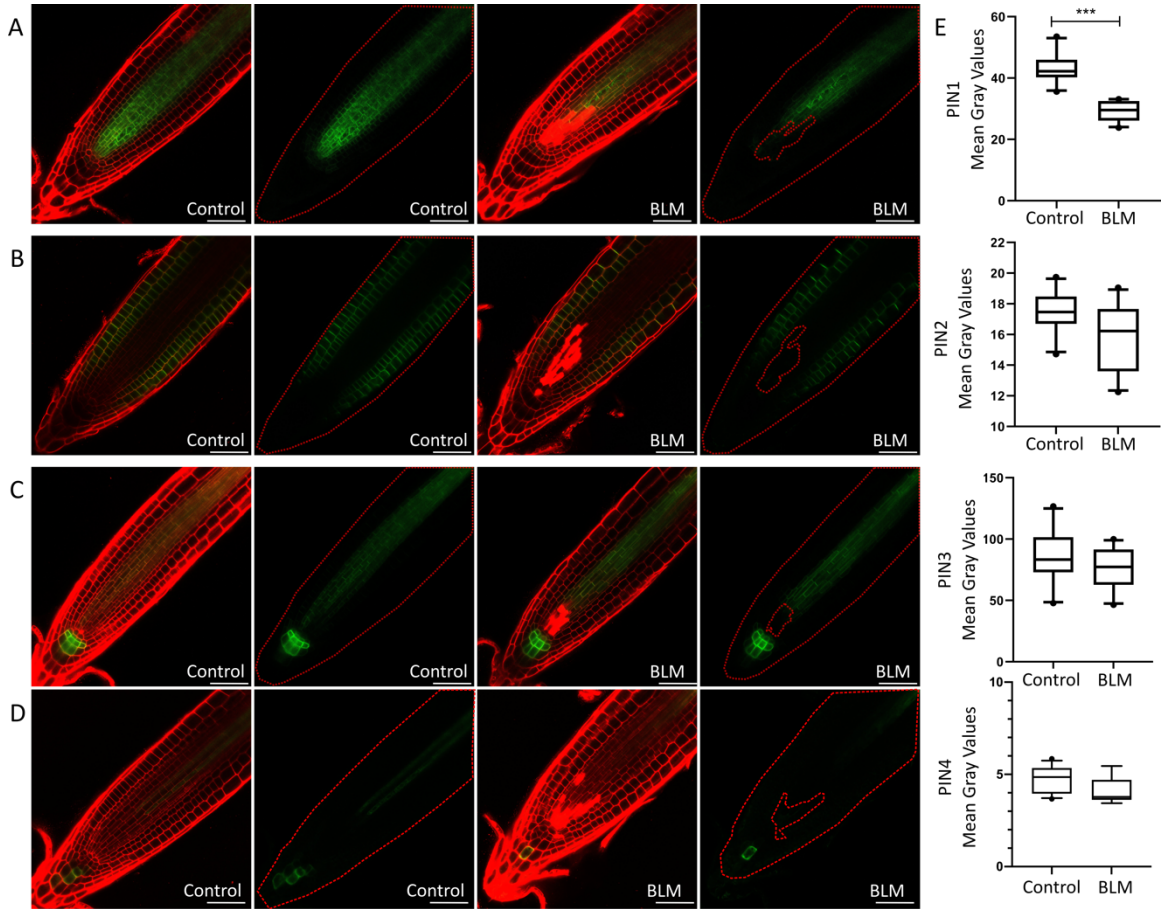


**Fig. S4.** (A,B,C) Confocal images of PIN1 (A), PIN2 (B), PIN3 (C), and PIN4 (D) translational GFP fusion reporter lines with or without 24 h of BLM treatment. Scale bars = 50 μm. (D) Quantification of GFP signal intensity from confocal images of PIN1, PIN2, PIN3, PIN4 translational reporter lines. (***, P<0.001).

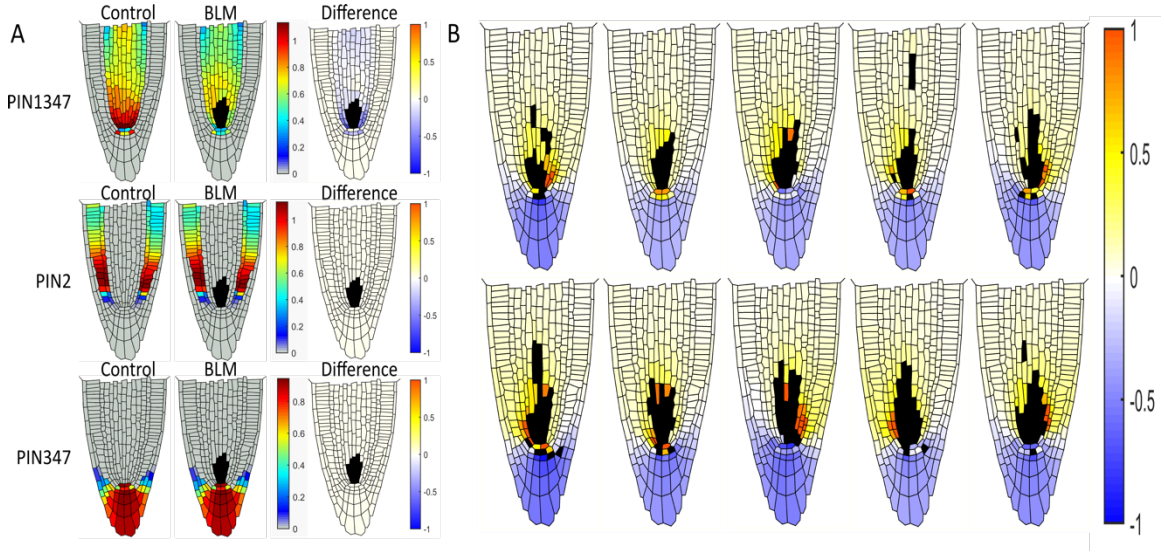


**Fig. S5.** (A,B) The steady-state model solutions for 2D cell layouts simulating the root meristem with and without BLM treatment. (A) PIN1347, PIN2 and PIN347 distributions. (B) Steady-state solutions for ten different cell death layouts corresponding to experimentally observed damages from BLM treatment. Yellow colors correspond to auxin accumulation, blue colors correspond to auxin reduction. Black areas correspond to the dead cells.

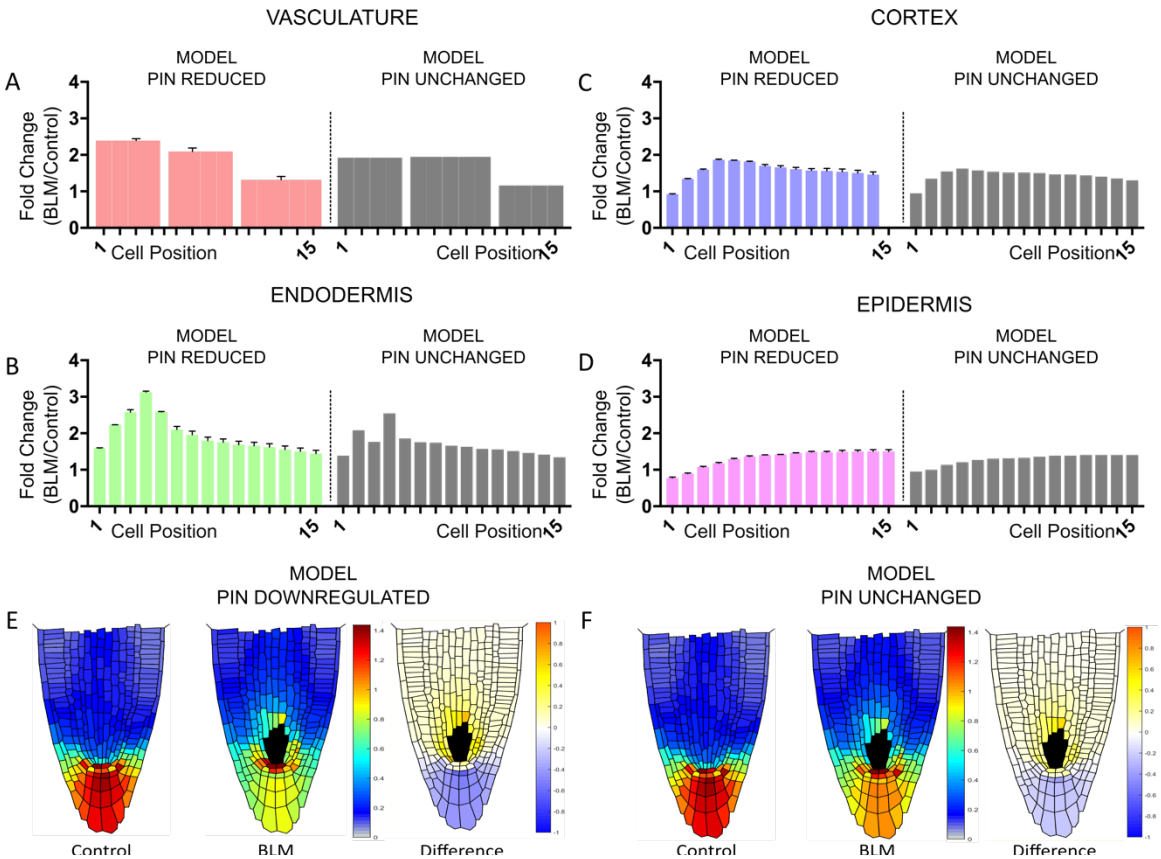


**Fig. S6.** (A,B) Side by side comparison of fold changes in auxin distributions (BLM vs Control) per tissue against distance from the QC (1 being the closest to QC) obtained from *in silico* modeling assuming downregulation (PIN REDUCED) or no change (PIN UNCHANGED) in PIN levels . Plots (A) and pictures (B) represents the average obtained from simulation of 10 real life cell death patterns. Error bars represent maximal errors calculated as described in methods. Colors correspond to auxin accumulation, blue colors correspond to auxin reduction. Black areas correspond to the dead cells.

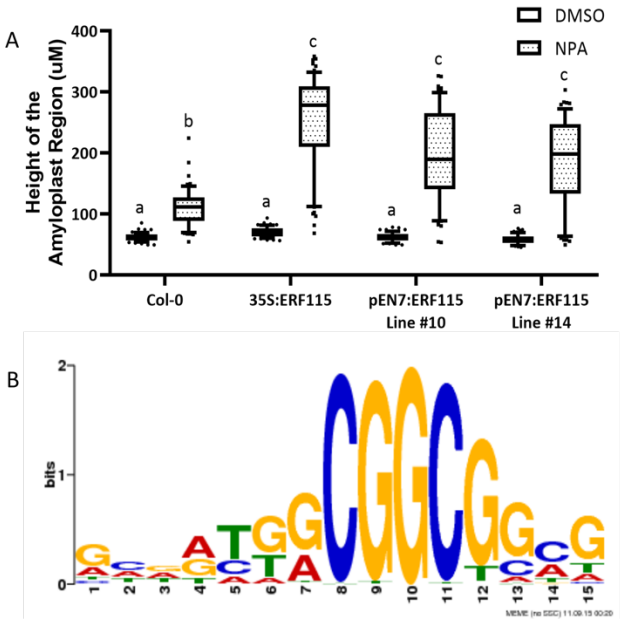


**Fig. S7.** (A) Quantification of the amyloplast-accumulating region height upon growth on DMSO or NPA for five days. All figures represent data acquired over three independent experiments. Statistical analysis was performed using mixed model analysis with least squares post-hoc tests and corrected for multiple pairwise comparisons using the Tukey method. Different letters represent statistical difference (a = P<0.005, b = P<0.05, c = P<0.01). (B) The logo for ERF115 binding region Position Weight Matrix (PWM) according to O'Malley *et al*. (11).

**Table S1. Parameter settings used in the mathematical model**

| Parameter | Symbol | Units | Value |
|---|---|---|---|
| The intensity of auxin flow from the upper root part | $k_\alpha$ | *mu/tu* | 0.55 |
| The degradation rate constant for PIN1347 | $K_{d,PIN1347}$ | *vu/tu* | 1000/600-870*/1000** |
| The degradation rate constant for PIN2 | $K_{d,PIN2}$ | *vu/tu* | 1000 |
| The degradation rate constant for PIN347 | $K_{d,PIN347}$ | *vu/tu* | 1000 |
| The degradation rate constant for auxin | $K_{d,a}$ | *vu/tu* | 0,005 |
| The synthesis rate constant for PIN1347 | $K_{s,PIN1347}$ | *mu/tu* | 1000 |
| The synthesis rate constant for PIN2 | $K_{s,PIN2}$ | *mu/tu* | 1000 |
| The synthesis rate constant for PIN347 | $K_{s,PIN347}$ | *mu/tu* | 1000 |
| The synthesis rate constant for auxin | $K_{s,a}$ | *mu/tu* | 0,002/0*** |
| The diffusion transport rate constant | $D$ | *lu/tu* | 0,08 |
| The activation thresholds of auxin-dependent synthesis of PIN1347 | $q_{1,PIN1347}$ | *1/cu* | 0,12 |
| The saturation thresholds for auxin-dependent synthesis of PIN1347 | $q_{2,PIN1347}$ | *1/cu* | 0,13 |
| The thresholds of auxin-dependent degradation of PIN1347 | $q_{3,PIN1347}$ | *1/cu* | 1,2 |
| The Hill coefficient, which determines the rate of PIN1347 synthesis in response to changes in intracellular auxin concentration | $s_{PIN1347}$ | *dl* | 2 |
| The coefficient that defines non-linearity of auxin-regulated PIN1347 degradation | $h_{PIN1347}$ | *dl* | 6 |
| The parameters of auxin-dependent synthesis and degradation for PIN2 | $q_{1,PIN2}$ | *1/cu* | 0,1 |
| | $q_{2,PIN2}$ | *1/cu* | 0,14 |
| | $q_{3,PIN2}$ | *1/cu* | 0,3 |
| | $s_{PIN2}$ | *dl* | 2 |
| | $h_{PIN2}$ | *dl* | 4 |
| The parameters of auxin-dependent synthesis and degradation for PIN347 | $q_{1,PIN347}$ | *1/cu* | 0,9 |
| | $q_{2,PIN347}$ | *1/cu* | 0,9 |
| | $s_{PIN347}$ | *dl* | 6 |

*mu* is the mass units, *cu* is concentration units, *tu* is the time units, *vu* is the volume units, *lu* is the length units, *dl* denotes the dimensionless parameter.

* for the Control / BLM treatment, when PIN1347 affected,

** for the Control / BLM treatment, when PINs are unaffected

*** for the QC and CSC / Other cell types

**Table S2.** Primers used in this study.

| **Primers Name** | **Sequence** |
|---|---|
| qCAK_F | ACCACCATTAACGTGCGTCAAC |
| qCAK_R | GATCTTGGCGAGAGAATCGGTATC |
| qACT2_F | AAAGGCCAACAGAGAGAAGA |
| qACT2_R | AGGATGGCATGAGGAAGAGA |
| qEMB2386_F | CTCTCGTTCCAGAGCTCGCAAAA |
| qEMB2386_R | AAGAACACGCATCCTACGCATCC |
| qWOX5_F | AGGCTAGGGAGAGGCAGAAA |
| qWOX5_R | CACCGGAAAGAGTTGTAATGT |
| qMP_FW | CCCAGGATTCTTCAGCTGTTGTG |
| qMP_REV | GCTGCATCAAGGGACTGAACTG |

**Table S3** Enrichment analysis for ARF5/MP binding sites among BLM induced and repressed genes. ARF5 binding sites were obtained from O'Malley *et al*. (11) and enrichment was tested using Fisher's exact test.

| | No of Genes with ARF5 binding site | Total No of Genes (FDR<0.05) | Ratio (%) | P Value (Fisher's exact test relative to unresponsive) |
|---|---|---|---|---|
| BLM Induced | 452 | 1071 | 0,422035481 | 0,04447 |
| Not induced | 7074 | 18845 | 0,375378084 | |
| | No of Genes with ARF5 binding site | Total No of Genes (FDR<0.05) | Ratio (%) | P Value (Fisher's exact test (relative to unresponsive) |
| BLM Repressed | 975 | 2778 | 0,350971922 | 0,03345 |
| Not repressed | 6551 | 17138 | 0,382249971 | |
| Total | 7526 | 19916 | 0,377887126 | |

**Movie S1 (separate file).** Time-lapse movie of the R2D2 reporter line stained with SR2200 dye during BLM treatment. The seedling was pre-treated with BLM for 8 h before imaging was started. The root tip tracking algorithm used here was described previously (12).

**Movie S2 (separate file).** Time-lapse movie of the PI-stained R2D2 reporter line during BLM treatment. The seedling was pre-treated with BLM for 10 h before imaging was started. The root tip tracking algorithm used here was described previously (12).

**Dataset S1 (separate file).** RNA-Seq Dataset containing gene expression and fold changes in Arabidopsis root tips upon BLM treatment

**References**


1. R. Patro, G. Duggal, M. I. Love, R. A. Irizarry, C. Kingsford, Salmon provides fast and bias-aware quantification of transcript expression. *Nat Methods* **14**, 417-419 (2017).
2. C. Soneson, M. I. Love, M. D. Robinson, Differential analyses for RNA-seq: transcript-level estimates improve gene-level inferences. *F1000Res* **4**, 1521 (2015).
3. M. I. Love, W. Huber, S. Anders, Moderated estimation of fold change and dispersion for RNA-seq data with DESeq2. *Genome Biol* **15**, 550 (2014).
4. Y. Benjamini, Y. Hochberg, Controlling the False Discovery Rate - a Practical and Powerful Approach to Multiple Testing. *J R Stat Soc B* **57**, 289-300 (1995).
5. I. De Smet *et al.*, An easy and versatile embedding method for transverse sections. *J. Microsc.* **213**, 76-80 (2004).
6. M. Savina, V. V. Mironova, PlantLayout pipeline to model tissue patterning *Vavilov Journal of Genetics and Breeding* **24**, 102-107 (2019).
7. J. H. Hong *et al.*, A Sacrifice-for-Survival Mechanism Protects Root Stem Cell Niche from Chilling Stress. *Cell* **170**, 102-113 e114 (2017).
8. V. V. Mironova *et al.*, Combined in silico/in vivo analysis of mechanisms providing for root apical meristem self-organization and maintenance. *Ann Bot* **110**, 349-360 (2012).
9. K. Bialek, J. D. Cohen, Quantitation of Indoleacetic-Acid Conjugates in Bean-Seeds by Direct Tissue Hydrolysis. *Plant Physiology* **90**, 398-400 (1989).
10. H. Schlenk, J. L. Gellerman, Esterification of Fatty Acids with Diazomethane on a Small Scale. *Anal Chem* **32**, 1412-1414 (1960).
11. R. C. O'Malley *et al.*, Cistrome and Epicistrome Features Shape the Regulatory DNA Landscape. *Cell* **165**, 1280-1292 (2016).
12. J. Heyman *et al.*, The heterodimeric transcription factor complex ERF115-PAT1 grants regeneration competence. *Nat Plants* **2**, 16165 (2016).